Supplemental Material: Theory of enhanced interlayer tunneling in optically driven high T_c superconductors

Jun-ichi Okamoto,[1,2,*] Andrea Cavalleri,[3,4] and Ludwig Mathey[1,2]

[1] *Zentrum für Optische Quantentechnologien and Institut für Laserphysik, Universität Hamburg, 22761 Hamburg, Germany*

[2] *The Hamburg Centre for Ultrafast Imaging, Luruper Chaussee 149, 22761 Hamburg, Germany*

[3] *Max Planck Institute for the Structure and Dynamics of Matter, 22761 Hamburg, Germany*

[4] *Department of Physics, Clarendon Laboratory, University of Oxford, Oxford OX1 3PU, UK*

I. EFFECTS OF HIGHER HARMONICS IN EQ. (2)

In this section, we discuss the effects of higher harmonics in Eq. (2) in the main text. The probing current I oscillates at a frequency $\omega_{\rm probe}$, and it is coupled to phases $\varphi_n \equiv \varphi(\omega_{\rm probe}+n\omega_{\rm pump})$ for an arbitrary integer n. To calculate the conductivity and the effective Josephson coupling, we need to know $\varphi_0 \equiv \varphi(\omega_{\rm probe})$ by solving the set of equations

$$\omega_{\rm Jp}^{-2} K_n \varphi_n = -\varphi_n - \frac{A}{2}\left(\varphi_{n-1}+\varphi_{n+1}\right) + \tilde{I}_{\rm probe}\delta_{n0}, \tag{1}$$

with $K_n = -(\omega_{\rm probe}+n\omega_{\rm pump})^2 - i\gamma(\omega_{\rm probe}+n\omega_{\rm pump})$. Approximately we can solve these linear equations by ignoring $\varphi_{m>|n|}$ and $\varphi_{m<-|n|}$ for a chosen integer n. Here we use $n=\pm1, 2$ and 5, and the obtained Josephson coupling as a function of the driving frequency $\omega_{\rm pump}$ is plotted in Fig. 1 for $A=0.4$ and 0.9 with $\gamma=0.05$. At $A=0.4$, the basic features around $\omega_{\rm pump}\sim\omega_{\rm Jp}$ are well converged already at $n=1$, while the higher harmonics create structures at lower harmonics $\omega_{\rm pump}\sim\omega_{\rm Jp}/2$ for $A=0.9$.

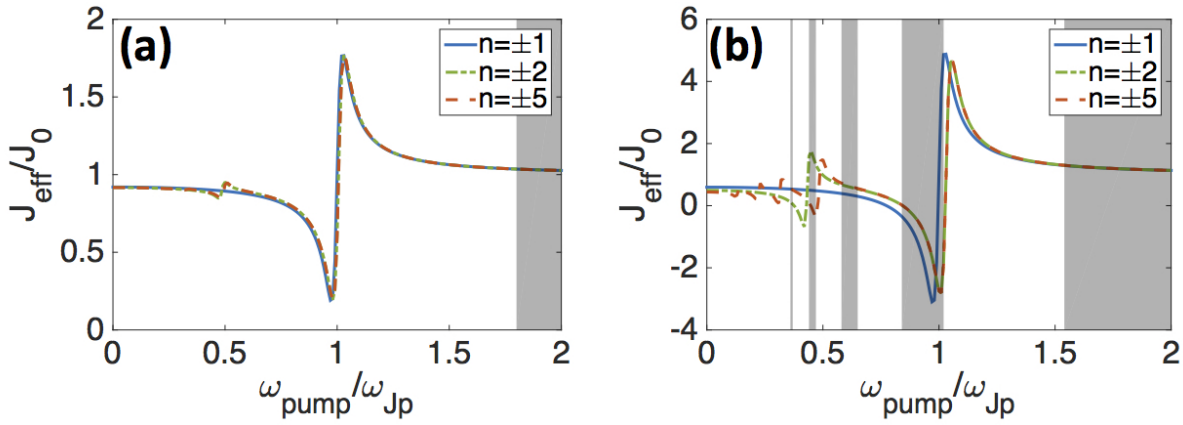

FIG. 1: (a) $J_{\rm eff}/J_0$ at $A=0.4$ for cases including up to $n=\pm1, 2$, and 5. (b) $J_{\rm eff}/J_0$ at $A=0.9$. Dynamically unstable regions are indicated by shaded regions.

II. FLOQUET STABILITY ANALYSIS

Here we briefly explain the Floquet stability analysis[1,2]. According to the Floquet theorem, a first order, linear differential equation

$$\dot{\vec{z}} = \mathbf{A}(t)\vec{z}, \tag{2}$$

with a periodic coefficient matrix $\mathbf{A}(t) = \mathbf{A}(t+T)$ has a solution in a form

$$z_i(t) = e^{(\ln \lambda_i)t/T} p_i(t) \tag{3}$$

with $\vec{p}(t) = \vec{p}(t+T)$. Here λ_i is an eigenvalue of the natural fundamental matrix $\mathbf{X}(T)$ given by the solutions of

$$\dot{\mathbf{X}} = \mathbf{A}(t)\mathbf{X} \tag{4}$$

with initial conditions $X(0) = \mathbf{1}$. If any absolute values of λ is bigger than 1, Eq. (3) is diverging, indicating dynamical instability.

In our model, we numerically solved the linearized equation of motion

$$\frac{d}{dt}\begin{bmatrix}\varphi \\ \dot{\varphi}\end{bmatrix} = \begin{bmatrix}\dot{\varphi} \\ -\gamma\dot{\varphi} - \omega_{\rm Jp}^2\left[1 + A\cos(\omega_{\rm pump}t)\right]\varphi\end{bmatrix}, \tag{5}$$

with initial conditions $(\varphi, \dot{\varphi}) = (1, 0)$ and $(0, 1)$ from $t = 0$ to $t = 2\pi/\omega_{\rm pump}$ to find the eigenvalues λ of the natural fundamental matrix.

III. NONLINEAR EFFECTS ON EQ. (1), AND LOSS FUNCTIONS

We consider the nonlinear effects in Eq. (1) in the main text. Its Fourier transformation leads to

$$(-\omega^2 - i\gamma\omega)\varphi(\omega) = \int \frac{d\omega'}{2\pi} M(\omega - \omega')\left[\sin\varphi\right]_{\omega'} + \tilde{I}(\omega), \tag{6}$$

where $M(\omega)$ is the Fourier transform of $M(t) = -\omega_{\rm Jp}^2[1 + A\cos(\omega_{\rm pump}t)]$. To see the nonlinear effect at the lowest order, we approximate $\sin\varphi \simeq \varphi - \varphi^3/3!$, and use the mean-field decompositions as [again, we limit ourselves to $\varphi(\omega_{\rm probe} \pm \omega_{\rm pump}) \equiv \varphi_{\pm1}$ and $\varphi(\omega_{\rm pump}) \equiv \varphi_0$]

$$\left[\sin\varphi\right]_{\omega_{\rm probe}} \simeq \varphi_0\left[1 - \left\langle\frac{1}{2}|\varphi_0|^2 + |\varphi_{-1}|^2 + |\varphi_{-1}|^2\right\rangle\right], \tag{7}$$

$$\left[\sin\varphi\right]_{\omega_{\rm probe}\pm\omega_{\rm pump}} \simeq \varphi_{\pm1}\left[1 - \left\langle\frac{1}{2}|\varphi_{\pm1}|^2 + |\varphi_0|^2 + |\varphi_{\mp1}|^2\right\rangle\right]. \tag{8}$$

We then have a set of equations, which needs to be solved self-consistently,

$$\begin{bmatrix}K_1 & 0 & 0 \\ 0 & K_0 & 0 \\ 0 & 0 & K_{-1}\end{bmatrix}\begin{bmatrix}\varphi_1 \\ \varphi_0 \\ \varphi_{-1}\end{bmatrix} = -\omega_{\rm Jp}^2\begin{bmatrix}1 & A/2 & 0 \\ A/2 & 1 & A/2 \\ 0 & A/2 & 1\end{bmatrix}\begin{bmatrix}\tilde{\varphi}_1 \\ \tilde{\varphi}_0 \\ \tilde{\varphi}_{-1}\end{bmatrix} + \begin{bmatrix}0 \\ \tilde{I} \\ 0\end{bmatrix}, \tag{9}$$

where $K_n = -(\omega_{\rm probe} + n\omega_{\rm pump})^2 - i\gamma(\omega_{\rm probe} + n\omega_{\rm pump})$, $\tilde{\varphi}_n = \varphi_n(1 - V_n)$, and V_n is the mean-field term expressed by angle brackets in Eqs. (3) and (4). We start from $V_n = 0$, and solve the above equations to get φ. Then we use this value to get new value of V_n, and then solve the equations again. We repeat the procedures until we get a converged result. We compare the effective Josephson coupling in Fig. 2 for linear and nonlinear models. For a linear model, we find unphysical regions where $J_{\rm eff}$ becomes negative, which disappear in the nonlinear model. The enhancement of Josephson coupling above $\omega_{\rm Jp}$ is bigger in the linear model than the nonlinear model. These observations comes from the fact that the diverging behavior $\varphi \sim (\omega_{\rm pump}^2 - \omega_{\rm Jp}^2)^{-1}$ is less pronounced in the nonlinear model, since the mean-field terms in Eqs. (3) and (4) reduce the amplitude of φ's once they become large.

The loss function is measured similarly by the probing current, and is defined as

$$L(\omega_{\rm probe}) \equiv -\,{\rm Im}[\omega_{\rm probe}/4\pi i\sigma(\omega_{\rm probe})] \propto {\rm Im}[\varphi(\omega_{\rm probe})/\tilde{I}_{\rm probe}]. \tag{10}$$

In Fig. 3, we compare the loss functions for linear and nonlinear models. $L(\omega_{\rm probe})$ shows a normal absorption peak around $\omega_{\rm probe} \simeq \omega_{\rm Jp}$. We also find a trough/peak around $\omega_{\rm pump} \simeq \omega_{\rm probe} \pm \omega_{\rm Jp}$, since, at these conditions, the parametric driving amplifies $\varphi(\omega_{\rm probe})$ through the mode $\varphi(\omega_{\rm probe} - \omega_{\rm pump})$. The sign of the loss function is determined by the phase difference between $\varphi(\omega_{\rm probe})$ and $\tilde{I}_{\rm probe}$. It is usually less than π as in a forced harmonic oscillator, and $L(\omega)$ is positive. However, for $\omega_{\rm pump} \simeq \omega_{\rm probe} + \omega_{\rm Jp}$, the phase difference becomes greater than π leading to negative values of $L(\omega)$. We note that a negative loss function near $\omega_{\rm pump} \simeq 2\omega_{\rm Jp}$ was observed in a LaBaCuO material in Ref. 3. In the linear model, we find an extra resonance around $\omega_{\rm pump} = -\omega_{\rm probe} + \omega_{\rm Jp}$, which disappears for the nonlinear case. Another nonlinear effect is the shift of resonance peak near $\omega_{\rm pump} \sim \omega_{\rm Jp}$; as the amplitude A becomes larger, the resonance frequency is pushed to lower frequencies [Fig. 3(d)]. We also find that the minimum of loss function near the dynamical instability is shifted to lower $\omega_{\rm pump}$ in the nonlinear case as the amplitude gets larger.

IV. EFFECT OF γ FOR EQS. (10) AND (11)

Here we give detailed expressions including the effect of damping γ for Eqs. (10) and (11) in the main text. Expanding the lengthy analytical solutions (obtained by considering three

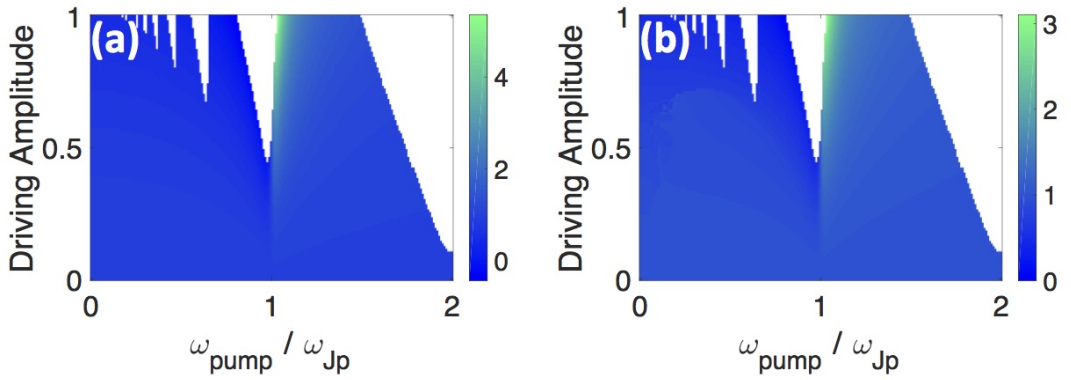

FIG. 2: Superfluid density without nonlinear effects (a) and with nonlinear effects (b). Dynamically unstable regions are excluded.

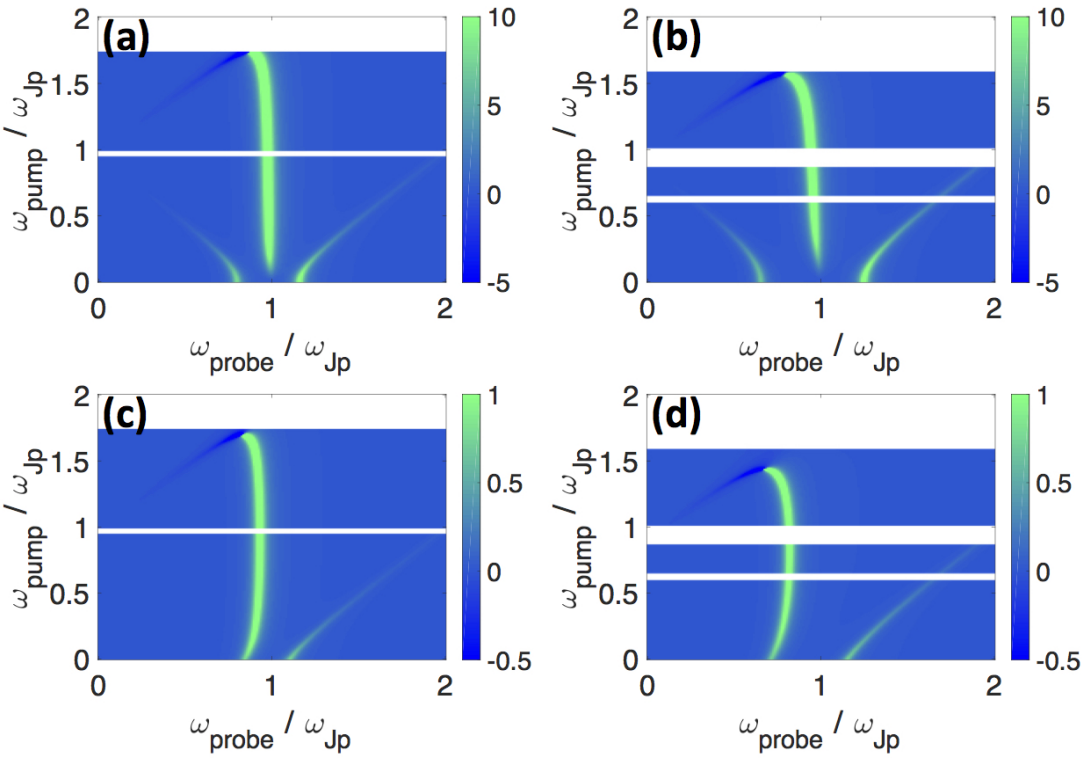

FIG. 3: (a), (b): Loss functions for a linear model at $A = 0.5$ and $A = 0.8$. (c), (d): Loss functions for a nonlinear model at $A = 0.5$ and $A = 0.8$. Dynamically unstable regions are excluded.

harmonics) by $A_{1,2} \sim 0$ and $\gamma \simeq 0$, near the lower resonance, $\omega_{\rm pump} \simeq \omega_{\rm Jp1}$, we have

$$\delta J/J_0 \simeq \frac{A_1^2 \omega_{\rm Jp1}^2}{2(\omega_{\rm pump}^2 - \omega_{\rm Jp1}^2)} \left[(1 + 2\alpha_1 + 2\alpha_2) + \frac{\omega_{\rm Jp1}^2 (2\alpha_2 + 1)^2}{(\omega_{\rm pump}^2 - \omega_{\rm Jp1}^2)^2} \gamma^2 \right] + \mathcal{O}(\omega_{\rm Jp1}/\omega_{\rm Jp2}). \quad (11)$$

This still diverges at $\omega_{\rm pump} = \omega_{\rm Jp1}$ since we treat γ perturbatively. Near the higher resonance $\omega_{\rm pump} \simeq \omega_{\rm Jp2}$, we have

$$\delta J/J_0 \simeq \frac{-2\alpha_2^2 A_1^2 + \alpha_1(1+2\alpha_2)A_2^2 + 4\alpha_1\alpha_2 A_1 A_2}{2\alpha_2(\omega_{\rm pump}^2 - \omega_{\rm Jp2}^2)}\Omega_1^2 - \frac{\alpha_1\left(2\alpha_2+1\right)A_2^2 + 4\alpha_1\alpha_2 A_1 A_2 + 4\alpha_2^2\left[\alpha_1\left(1-2\alpha_2\right) - 2\alpha_2^2\right]A_1^2}{2\alpha_2(\omega_{\rm pump}^2 - \omega_{\rm Jp2}^2)^3}\Omega_1^2\Omega_2^2\gamma^2 + \mathcal{O}(\omega_{\rm Jp1}/\omega_{\rm Jp2}). \tag{12}$$

V. COUPLED SINE-GORDON EQUATIONS WITH LANGEVIN NOISES

Here we show the details of the coupled sine-Gordon equation used for our simulations. The starting Hamilton equations, based on the Hamiltonian in Eq. (6) in the main text, are[12]

$$\begin{aligned}\left(\frac{\hbar}{e^*}\right)\dot{\theta}_m &= \sum_n \frac{1}{2C_{\rm av}}\left(-\frac{|x_m - x_n|}{d} + 2\kappa\delta_{mn}\right)Q_n, \\ \left(\frac{\hbar}{e^*}\right)\dot{Q}_m &= \frac{\hbar W}{e^*}\left[j_m^{m+1}\sin\varphi_{m+1,m} - j_{m-1}^m \sin\varphi_{m,m-1}\right],\end{aligned} \tag{13}$$

where we introduced a phase difference between the mth and $(m+1)$th SC layers as $\varphi_{m+1,m} = \theta_{m+1} - \theta_m$. Eliminating $\{Q_m\}$ leads to the coupled sine-Gordon equations derived in Refs. 4 and 5

$$\ddot{\vec{\varphi}} \equiv \begin{bmatrix}\ddot{\varphi}_{10}\\ \ddot{\varphi}_{21}\\ \ddot{\varphi}_{32}\\ \vdots\end{bmatrix} = \begin{bmatrix}-(1+2\alpha_1)\Omega_1^2 & \alpha_2\Omega_2^2 & & \\ \alpha_1\Omega_1^2 & -(1+2\alpha_2)\Omega_2^2 & \alpha_1\Omega_1^2 & \\ & \alpha_2\Omega_2^2 & -(1+2\alpha_1)\Omega_1^2 & \alpha_2\Omega_2^2 \\ & & \ddots & \end{bmatrix}\begin{bmatrix}\sin\varphi_{10}\\ \sin\varphi_{21}\\ \sin\varphi_{32}\\ \vdots\end{bmatrix} \equiv \mathbf{M}\vec{J_s} \tag{14}$$

where α_i is the capacitive coupling constant

$$\alpha_i = \epsilon_i \mu^2/sd_i, \tag{15}$$

and Ω_i is the bare plasma frequency of a junction,

$$\Omega_i = \sqrt{\frac{4\pi e^* d_i j_i}{\hbar\epsilon_i}}. \tag{16}$$

We further add the damping term γ, Langevin thermal noises $\vec{\xi}$, a total external current $I(t)$,

$$\ddot{\vec{\varphi}} + \gamma\dot{\vec{\varphi}} = \mathbf{M}\vec{J_s} + \vec{I_0} + \vec{\xi}, \tag{17}$$

where $\vec{I_0} = 4\pi e^*\mu^2 I/s\hbar(\alpha_1^{-1}, \alpha_2^{-1}, \alpha_1^{-1}, \dots)$. The Langevin noises are correlated as $\langle\xi_i(t)\xi_j(t')\rangle = \delta(t-t')2\gamma c^2 k_B T B_{ij}$ where B_{ij} is the (i,j) component of a matrix $\mathbf{B}$,

$$\mathbf{B} = \frac{16\pi^3\mu^2}{\phi_0^2 W s}\begin{bmatrix} 2+\alpha_1^{-1} & -1 & & & \\ -1 & 2+\alpha_2^{-1} & -1 & & \\ & -1 & 2+\alpha_1^{-1} & -1 & \\ & & & \ddots & \end{bmatrix}, \tag{18}$$

k_B is the Boltzman constant and $\phi_0 = hc/e^*$ is the flux quantum. For the simulations, we normalize the temperature by $\hbar j_1 W/\alpha_1\Omega_1^2 e^*$.

Response functions can be calculated using an external current $I(t) = I_0\cos(\omega_{\rm pump}t)$, and the voltage response $V(t)$ as discussed in Ref. 6. The voltage is related to the phase differences by generalized Josephson relations:

$$\left(\frac{\hbar}{e^*}\right)\dot{\vec{\varphi}} = \mathbf{\Lambda}\vec{V} \tag{19}$$

with

$$\mathbf{\Lambda} = \begin{bmatrix} 1+2\alpha_1 & -\alpha_2 & & & \\ -\alpha_1 & 1+2\alpha_2 & -\alpha_1 & & \\ & -\alpha_2 & 1+2\alpha_1 & -\alpha_2 & \\ & & & \ddots & \end{bmatrix}. \tag{20}$$

The average electric field for the whole junctions is $E_{\rm av}(t) = V(t)/(dN)$. The numerically obtained response functions are plotted in Fig. 4. For an unperturbed case, the conductivity of a linear model can be calculated analytically at $T = 0$,

$$\sigma(\omega) = \frac{\epsilon_{\rm av}}{4\pi i}\frac{\left(\omega^2 + i\gamma\omega - \omega_{\rm Jp1}^2\right)\left(\omega^2 + i\gamma\omega - \omega_{\rm Jp2}^2\right)}{\omega\left(\omega^2 + i\gamma\omega - \omega_t^2\right)}, \tag{21}$$

where $\omega_{\rm Jp1,\ Jp2}$ are two longitudinal plasma modes

$$\omega_{\rm Jp1,\ Jp2}^2 = \left(\frac{1}{2}+\alpha_1\right)\Omega_1^2 + \left(\frac{1}{2}+\alpha_2\right)\Omega_2^2 \mp \sqrt{\left[\left(\frac{1}{2}+\alpha_1\right)\Omega_1^2 - \left(\frac{1}{2}+\alpha_2\right)\Omega_2^2\right]^2 + 4\alpha_1\alpha_2\Omega_1^2\Omega_2^2}, \tag{22}$$

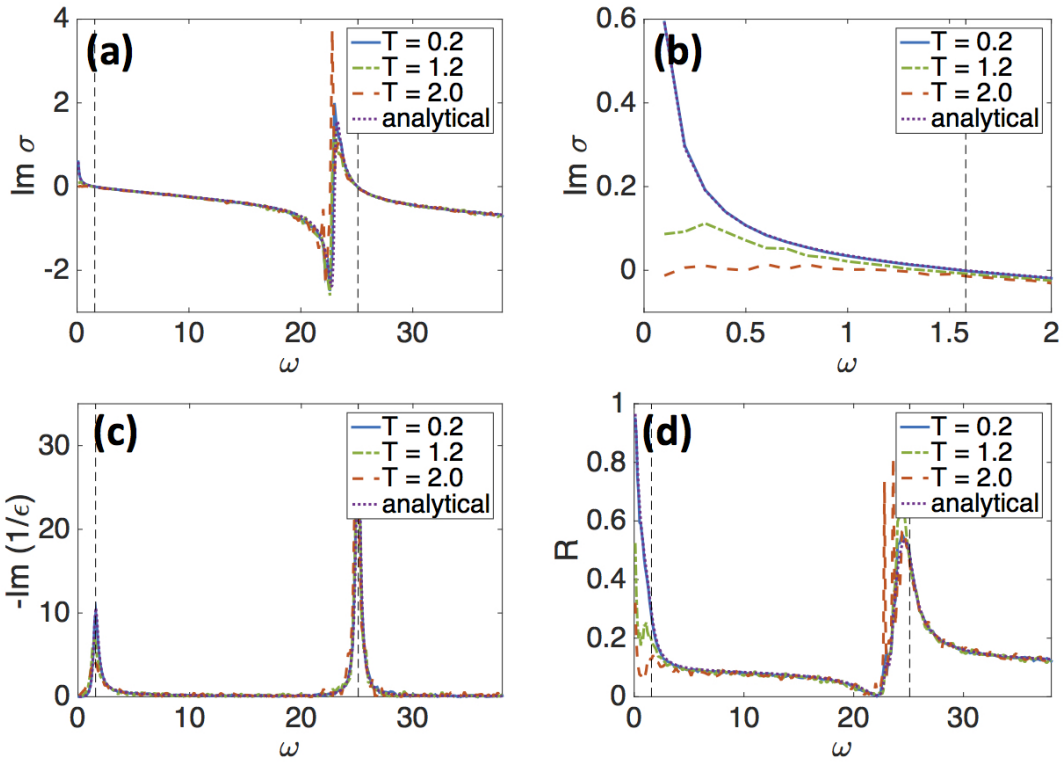

FIG. 4: (a) Imaginary part of conductivity, (b) A closer look of (a) near $\omega_{\mathrm{Jp1}} = 1.58$, (c) loss function, and (d) reflectivity. $\epsilon_{\mathrm{av}} \approx 0.25$ in our unit.

and ω_t is the transverse plasma mode,

$$\omega_t^2 = \frac{1 + 2\alpha_1 + 2\alpha_2}{\alpha_1 + \alpha_2} \left(\alpha_1 \Omega_1^2 + \alpha_2 \Omega_2^2\right). \tag{23}$$

Fig. 4 (a) and (b) reproduce the basic features of this analytical solution such as the diverging behavior near ω_t, and $1/\omega$ divergence as $\omega \ll \omega_{\mathrm{Jp1}}$. As the temperature increases, the latter divergence, the signature of superconducting states, disappears around $T = 1.0$. Fig. 4 (c) shows the loss function, and the two peaks correspond to the absorption peaks of two plasma frequencies $\omega_{\mathrm{Jp1,\ Jp2}}$. Fig. 4 (d) is the reflectivity. While BCS type superconductors show perfect reflection $R \sim 1$ below the gap energy, in a layered compound R gets nearly 1 only at very low frequencies since the screening is not perfect.

VI. POWER SPECTRUM FOR A LINEARIZED MODEL: GREEN'S FUNCTION METHOD

Here we outline an approach to obtain power spectrum for a linearized model; Green's function method[1,7,8]. We consider $2N$ coupled parametrically driven Brownian oscillators that obeys the linearized equations of Eq. (17).

$$\ddot{\vec{\varphi}} + \gamma\dot{\vec{\varphi}} - \mathbf{M}(t,\phi)\vec{\varphi} = \vec{\xi}, \tag{24}$$

where $\langle \xi_i(t)\xi_j(s)\rangle = 2\gamma c^2 k_B T B_{ij}\delta(t-s)$, and the driving depends on the initial phase ϕ. Introducing a new variable $\vec{\varphi} = \vec{y}e^{-\frac{\gamma}{2}t}$, we get

$$\ddot{\vec{y}} - \mathbf{M}(t,\phi)\vec{y} - \frac{\gamma^2}{4}\mathbf{1}_n\vec{y} = \vec{\xi}e^{\frac{\gamma}{2}t} \equiv \vec{\eta}. \tag{25}$$

Now we make this second order differential equation into a first order equation by using $\vec{z} = (\vec{y}, \dot{\vec{y}})^t$. The equation of motion is found to be

$$\dot{\vec{z}} = \begin{bmatrix} 0 & \mathbf{1}_n \\ \mathbf{M}(t,\phi) + \mathbf{1}_n\frac{\gamma^2}{4} & 0 \end{bmatrix}\vec{z} + \begin{bmatrix} 0 \\ \vec{\eta} \end{bmatrix} \equiv \mathbf{A}(t,\phi)\vec{z} + \vec{f}(t). \tag{26}$$

The natural fundamental matrix $\mathbf{\Phi}(t,\phi)$ is numerically obtained by solving the equation with the initial condition $\mathbf{\Phi}(0) = \mathbf{1}_{2n}$ without the inhomogeneous term, i.e., $\dot{\mathbf{\Phi}} = \mathbf{A}(t,\phi)\mathbf{\Phi}$. The Green's matrix is defined as

$$\mathbf{G}(t,s,\phi) = \mathbf{\Phi}(t,\phi)\mathbf{\Phi}^{-1}(s,\phi). \tag{27}$$

Then the solution is given by[1]

$$\vec{z}(t,\phi) = \mathbf{\Phi}(t,\phi)\vec{z}(0) + \int_0^t \mathbf{G}(t,s,\phi)\vec{f}(s)ds \tag{28}$$

Going back to the original basis $\vec{\varphi}$, we need to be careful that $\dot{\vec{y}}(0) = \dot{\vec{\varphi}}(0) + \frac{\gamma}{2}\vec{\varphi}(0)$.

We focus on the homogeneous case, $\varphi_1 = \varphi_3 = \varphi_5 = \cdots$ and $\varphi_2 = \varphi_4 = \varphi_6 = \cdots$. The correlation function of the 1st junction is (for $t > t'$)

$$\begin{aligned}\langle\varphi_1(t,\phi)\varphi_1(t',\phi)\rangle = \sum_{i',j'=1}^{4}\Big[&\mathbf{\Phi}_{1i'}(t,\phi)z_{i'}(0)\mathbf{\Phi}_{1j'}(t',\phi)z_{j'}(0) \\ &+ 2\gamma k_B T\int_0^{t'}\mathbf{G}_{1i'}(t,s,\phi)\mathbf{G}_{1j'}(t',s,\phi)\tilde{\mathbf{B}}_{i'j'}e^{\gamma s}ds\Big]e^{-\frac{\gamma}{2}(t+t')},\end{aligned} \tag{29}$$

where $\vec{z}(0) = (\varphi_1(0), \varphi_2(0), \dot{\varphi}_1(0) + \frac{\gamma}{2}\varphi_1(0), \dot{\varphi}_2(0) + \frac{\gamma}{2}\varphi_2(0))$ and $\langle f_i(s) f_j(s') \rangle = 2\gamma c^2 k_B T \tilde{B}_{ij} \delta(s - s') e^{\gamma s}$ with

$$\tilde{\mathbf{B}} = \begin{bmatrix} 0 & 0 \\ 0 & \mathbf{B} \end{bmatrix}. \tag{30}$$

The upper limit of the integral is t' since we now consider $t > t'$. In the long-time limit, the steady state is expected to be independent of the initial condition, so we will focus on the second term. The time translation invariance will be recovered after averaging over the phase ϕ. The power spectrum at $\omega = 26$, $T = 0.6$, $A_1 = 1.0$, and $A_2 = 0.3$ is given in Fig. 5. We see that the spectral weights are reduced for low frequencies, while the total weights, i.e., the sum of weights over all frequencies, are increased. This basically agrees with the power spectrum obtained from Langevin simulations in the main text.

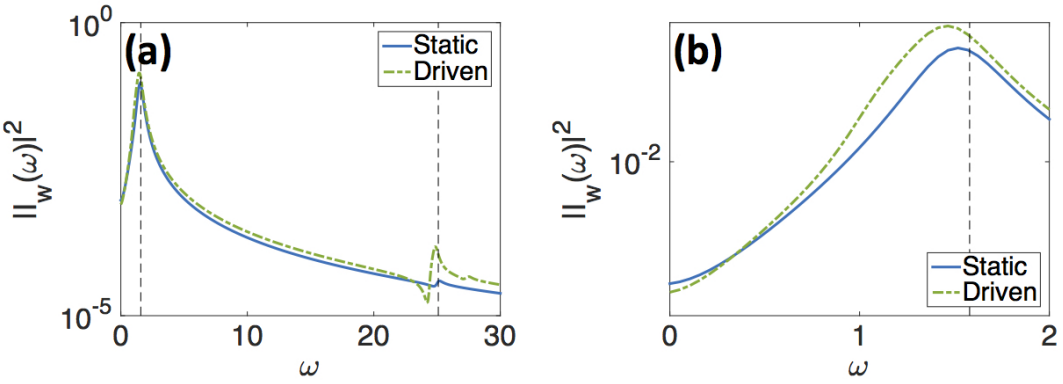

FIG. 5: Power spectrum of static and driven ($\omega_{\rm pump} = 26.0$) cases at $T = 0.6$ with $A_1 = 1.0$ and $A_2 = 0.3$. (a) a wide view (b) a closer view near $\omega_{\rm Jp1} = 1.58$.

VII. LINEAR RESPONSE THEORY

We summarize the linear response theory for bilayer Josephson junctions that obey the stochastic equations of motion in Eq. (17). The corresponding Fokker-Plank equation for a probability density $p(\vec{\varphi}, \dot{\vec{\varphi}}, t)$ is

$$\dot{p} = (\mathcal{L}_0 + \mathcal{L}_1) p, \tag{31}$$

where $\mathcal{L}_0$ is the unperturbed part

$$\begin{aligned}\mathcal{L}_0 = \gamma c^2 k_B T \sum_{ij} \left(B_{ij} \frac{\partial^2}{\partial\dot{\varphi}_i \partial\dot{\varphi}_j} \right) \\ + \sum_i \left[-\dot{\varphi}_i \frac{\partial}{\partial\varphi_i} + \frac{\partial}{\partial\dot{\varphi}_i} \left(\gamma\dot{\varphi}_i + \frac{c^2\hbar W}{e^*} \sum_j B_{ij} j_j \sin\varphi_j \right) \right],\end{aligned} \tag{32}$$

and $\mathcal{L}_1$ is the perturbation by the probing current

$$\mathcal{L}_1(t) = -\sum_i I_{0,i}(t) \frac{\partial}{\partial\dot{\varphi}_i}. \tag{33}$$

The deviation of a phase velocity from the equilibrium distributions is related to correlation functions[9]

$$\begin{aligned}\delta\langle\dot{\varphi}_i\rangle(t) &= \sum_j \int_{-\infty}^{\infty} ds R^{ij}(t-s) I_{0,j}(s), \\ R^{ij}(t) &= \frac{1}{c^2 k_B T} \sum_k B^{-1}_{jk} \langle\dot{\varphi}_i(t)\dot{\varphi}_k(0)\rangle,\end{aligned} \tag{34}$$

or equivalently $\delta\langle\dot{\varphi}_i\rangle(\omega) = \sum_j R^{ij}(\omega) I_{0,j}(\omega)$. Defining the velocity susceptibility as $\chi_{ij}(t) = \langle\dot{\varphi}_i(t)\dot{\varphi}_j(0)\rangle$, the total voltage difference is

$$\vec{V}(\omega) = \frac{\hbar}{e^* c^2 k_B T} \mathbf{\Lambda}^{-1} \chi(\omega) \mathbf{B}^{-1} \vec{I_0}(\omega). \tag{35}$$

Now for the sake of simplicity we consider spatially homogeneous case. The largest contribution to the voltage is from the weak junctions, so we can approximate the total voltage across the two junctions is

$$V(\omega) \simeq \frac{\hbar^2}{e^{*2} W k_B T} \chi_{11}(\omega) I(\omega). \tag{36}$$

Since the velocity susceptibility is connected to the coordinate susceptibility by the simple time derivative[9], this formula indicates that the lower power spectrum of the current fluctuations at low frequencies leads to a larger conductivity.

---

* Electronic address: ojunichi@physnet.uni-hamburg.de

[1] A. Coddington and R. Carlson, *Linear Ordinary Differential Equations* (Society for Industrial and Applied Mathematics, 1997).

[2] L. Cesari, *Asymptotic Behavior and Stability Problems in Ordinary Differential Equations*, Ergebnisse der Mathematik und ihrer Grenzgebiete. 2. Folge (Springer Berlin Heidelberg, 2012).

[3] S. Rajasekaran, E. Casandruc, Y. Laplace, D. Nicoletti, G. D. Gu, and S. R. Clark, arXiv:1511.08378.

[4] T. Koyama, J. Phys. Soc. Jpn. **71**, 2986 (2002).

[5] M. Machida and S. Sakai, Phys. Rev. B **70**, 144520 (2004).

[6] T. Koyama, J. Phys. Soc. Jpn. **70**, 2114 (2001).

[7] C. Zerbe, P. Jung, and P. Hänggi, Phys. Rev. E **49**, 3626 (1994).

[8] R. M. Mazo, J. Stat. Phys. **24**, 39 (1981).

[9] H. Risken and T. Frank, *The Fokker-Planck Equation: Methods of Solution and Applications*, Springer Series in Synergetics (Springer Berlin Heidelberg, 1996).

[10] D. van der Marel and A. A. Tsvetkov, Phys. Rev. B **64**, 024530 (2001).

[11] E. Šimánek, *Inhomogeneous Superconductors: Granular and Quantum Effects*, International series of monographs on physics (Oxford University Press, 1994).

[12] There is a difference between the capacitive matrix between Ref. 4, and Ref. 10, while the equations of motion are not affected by the difference. See p. 56 of Ref. 11.